HHS Public Access

Author manuscript

Glia. Author manuscript; available in PMC 2016 September 01.

Published in final edited form as:

Glia. 2015 September ; 63(9): 1646–1659. doi:10.1002/glia.22834.

Voltage-dependent K^+ currents contribute to heterogeneity of olfactory ensheathing cells

Lorena Rela[1,4,5], **Ana Paula Piantanida**[4,5], **Angelique Bordey**[1,3], and **Charles A. Greer**[1,2]

[1]Department of Neurosurgery, Yale University School of Medicine, New Haven, CT 06520

[2]Department of Neurobiology, Yale University School of Medicine, New Haven, CT 06520

[3]Department of Cellular and Molecular Physiology, Yale University School of Medicine, New Haven, CT 06520

[4]Systems Neuroscience Section, Department of Physiology and Biophysics, School of Medicine, University of Buenos Aires

[5]Institute of Physiology and Biophysics Bernardo Houssay (IFIBIO Houssay-CONICET), C1121ABG Buenos Aires, Argentina

Abstract

The olfactory nerve is permissive for axon growth throughout life. This has been attributed in part to the olfactory ensheathing glial cells that encompass the olfactory sensory neuron fascicles. Olfactory ensheathing cells also promote axon growth *in vitro* and when transplanted *in vivo* to sites of injury. The mechanisms involved remain largely unidentified owing in part to the limited knowledge of the physiological properties of ensheathing cells. Glial cells rely for many functions on the properties of the potassium channels expressed; however, those expressed in ensheathing cells are unknown. Here we show that olfactory ensheathing cells express voltage-dependent potassium currents compatible with inward rectifier (K_{ir}) and delayed rectifier (K_{DR}) channels. Together with gap junction coupling, these contribute to the heterogeneity of membrane properties observed in olfactory ensheathing cells. The relevance of K^+ currents expressed by ensheathing cells is discussed in relation to plasticity of the olfactory nerve.

Keywords

Ensheathing glia; potassium conductance; gap junctions

Introduction

Olfactory sensory neurons (OSNs) are generated throughout life (Caggiano et al. 1994; Graziadei and Graziadei 1979) and their axons within the olfactory nerve successfully reinnervate the olfactory bulb to maintain function and topography (Gogos et al. 2000;

Corresponding author: Charles A. Greer, Ph.D. Department of Neurosurgery, Yale University School of Medicine, P.O. Box 208082, New Haven, CT 06520-8082, Telephone – 203.785.4034, – charles.greer@yale.edu.

The authors declare no competing financial interests.

Harding and Wright 1979). The permissive nature of the olfactory nerve for axon growth has been attributed to olfactory ensheathing cells (OECs), specialized nonmyelinating glia associated with OSN axons (Doucette 1990; 1991). OECs express a unique combination of molecular markers including GFAP and S100B, expressed by astrocytes and Schwann cells, proteolipid protein (PLP), expressed by oligodendrocytes and Schwann cells, and brain lipid binding protein (BLBP), associated to radial glia (Feng et al. 1994; Griffiths et al. 1995; Hachem et al. 2005; Platel et al. 2009; Puckett et al. 1987; Rela et al. 2010).

Growth-associated molecules are expressed in the adult olfactory nerve (Kafitz and Greer 1998; Liesi 1985; Miragall et al. 1988; Ramakers et al. 1992; Reinhard et al. 1988) and are up-regulated after lesion (Turner and Perez-Polo 1993), however, the mechanisms underlying olfactory nerve plasticity remain largely unidentified. *In vitro* experiments showed that OECs promote axon growth when co-cultured with neurons (Kafitz and Greer 1999; Runyan and Phelps 2009), an effect modulated by intracellular calcium (Hayat et al. 2003) and perhaps mediated by brain derived neurotrophic factor (BDNF) (Runyan and Phelps 2009) and/or SCARB2 (Roet et al. 2013). OEC transplants can improve axonal regeneration in animal models of spinal cord or nerve injury, although the mechanisms are unclear and the effects often limited (Bartolomei and Greer 2000; Raisman et al. 2012; Schwab 2002). Clinical trials of OECs, though not without controversy (Dlouhy et al. 2014; Dobkin et al. 2006; Harrop et al. 2012), have produced some promising results (Feron et al. 2005; Huang et al. 2003; Lima et al. 2006; Mackay-Sim et al. 2008; Tabakow et al. 2014).

Characterizations of OECs properties *in vitro* and after transplant are more abundant than analyses within the olfactory nerve, where neurotrophic effects of OECs appear to be efficiently expressed. Addressing this gap in our knowledge will shed new light on the basic membrane properties of OECs and how they may contribute to the support of plasticity within the olfactory nerve. This issue is particularly significant given that OECs are inherently plastic and adopt different morphologies and molecular expression profiles *in vitro* (Alexander et al. 2002; Franceschini and Barnett 1996; Vincent et al. 2003) and *in vivo* (Akiyama et al. 2004; Dunning et al. 2004).

Although glial cells depend on K^+ channels for functions that may be relevant for the plasticity of the olfactory nerve such as regulation of the cell cycle (Chiu and Wilson 1989; MacFarlane and Sontheimer 2000) and migration (Tiwari-Woodruff et al. 2006), the properties of K^+ membrane conductance in OECs are unknown. Consequently, here we report on studies showing the profiles of K^+ membrane currents displayed by OECs in acute slices of the OB and their contribution to the heterogeneity observed in membrane properties of the OEC population (Rela et al. 2010).

Materials and Methods

Animals

Male and female CD-1 mice [postnatal day 14 (P14) to P21] (Charles River, Wilmington, MA) were housed in a 12/12 light cycle with water and food *ad libitum*. Mice were anesthetized with sodium pentobarbital (80 mg/kg, i.p.; Nembutal; Abbott Laboratories,

North Chicago, IL) before dissection. All procedures were approved by the Yale University Animal Care and Use Committee and conform to NIH guidelines.

Acute slice preparation

Horizontal brain slices were prepared as previously reported (Rela et al. 2010). Briefly, anesthetized mice were decapitated and the brain removed and chilled (0–4 °C) in 95% O_2-5% CO_2-saturated sucrose-based artificial cerebrospinal fluid (ACSF) containing (in mM): 220 Sucrose, 2.5 KCl, 1 $CaCl_2$, 6 $MgCl_2$, 1.25 NaH_2PO_4, 26 $NaHCO_3$ and 10 glucose. The brain was affixed with cyanoacrylate glue to a vibratome stage and 250μm slices were cut in cold oxygenated sucrose-based ACSF. The slices recovered at room temperature for >1 hour in ACSF containing (in mM): 125 NaCl, 2.5 KCl, 2 $CaCl_2$, 1.1 $MgCl_2$, 1.25 NaH_2PO_4, 26 $NaHCO_3$ and 10 glucose, pH 7.4. Slices were subsequently placed in a flow-through chamber, held in position by a harp (Warner Instruments, Hamden, CT), and superfused with oxygenated ACSF at room temperature. Voltage-clamp experiments were performed on an upright Olympus BX51WI microscope (Optical Analysis, Nashua, NH) equipped with Nomarski phase-contrast, water-immersion and fluorescence optics (60x; numerical aperture, 0.9), and infra-red illumination.

Electrophysiological recordings and drug applications

OECs not adjacent to blood vessels were visually identified in the olfactory nerve layer (ONL) where they constitute >95% of the cells (Au et al. 2002; Valverde and Lopez-Mascaraque 1991). Whole cell voltage-clamp recordings were obtained as previously described (Rela et al. 2010). Patch pipettes were pulled from thin-walled borosilicate glass (1.50/1.10mm outside/inside diameters, respectively; BF150-110-10; Sutter Instrument, Novato, CA) on a P-97 puller (Sutter). Pipette resistance was 5–10MΩ when filled with the following (in mM): 130 KCl, 0.25 $CaCl_2$, 4 $MgCl_2$, 5 ethylene glycol-bis-(aminoethyl ether)-*N*,*N*,*N*′,*N*′-tetraacetic acid (EGTA), 10 N-2-hydroxyethyl-piperazine-N′-2-ethanesulfonic acid (HEPES), 4 K_2ATP and 0.5 Na_2GTP. The pH was adjusted to 7.3 with KOH. Osmolarity was measured with a vapor pressure osmometer 5520 (Wescor, Logan, UT); the intracellular and extracellular solutions were 295–300 and 305–310mOsm, respectively. Lucifer Yellow (LY, dilithium salt, Invitrogen/Molecular Probes, 0.1%) was added to the pipette solution to confirm the identity of OECs (high resistance pipettes increase the efficiency of pipette withdrawal, preserving cell integrity). Whole cell recordings were performed using a MultiClamp 700B amplifier (Molecular Devices, Sunnyvale, CA). Current signals were low-pass filtered at 4kHz and digitized at 10kHz using a Digidata 1440A digitizing board (Molecular Devices) with a Dell computer system. Data acquisition, storage, and analysis were done using PClamp version 10 (Molecular Devices). Capacitance and series resistance compensation (at least 60%) were used to minimize voltage errors. Settings were determined by compensating the transients of a small (10mV) 50ms hyperpolarizing voltage step. The capacitance reading of the amplifier was used as the value for whole cell capacitance. Leak conductance was not subtracted. Resting potential (V_r) was measured after switching to zero-current mode. Barium Chloride (Ba^{2+}, 100μM), Tetraethylammonium (TEA, 20mM) and Meclofenamic acid (MFA, 100μM), were diluted in ACSF and applied through a rapid bath application system. OECs were assigned randomly to each treatment. Chemicals were purchased from Sigma Chemical Co. (St.

Louis, MO), unless otherwise noted. The location of OECs in the ONL was determined after recording as the distance of the recording pipette tip to the inner ONL border (the border between the ONL and the glomerular layer of the OB) under DIC illumination at low magnification (Figure 7A1).

Immunohistochemistry

To assess connexin43 (Cx43) immunoreactivity the acute OB slices were post-fixed overnight with 4% paraformaldehyde in phosphate buffered saline (PBS 0.1M). The tissue was blocked for 2 hours in PBS containing 2% bovine serum albumin and 0.3% Triton X-100 (American Bioanalytical, Natick, MA). The primary antibody (rabbit antiCx43 71–0700; Invitrogen/Life Technologies, Grand Island, NY) was diluted 1:500 in blocking buffer and incubated overnight at room temperature. Sections were washed 3 times in 0.3% Triton X-100 in PBS for 10 minutes and incubated in secondary antibodies conjugated to Alexa Fluor (Invitrogen/Life Technologies, Grand Island, NY) and the nuclear marker DRAQ5 (Alexis Biochemicals, San Diego, CA), all diluted 1:1000 in blocking buffer for 2 hours at room temperature. Sections were washed as above, rinsed in PBS, mounted in Gel-Mount and coverslipped. Images were acquired with a Leica confocal microscope as z-stacks, with 1μm steps between optical sections, using an oil-immersion objective (40X; numerical aperture, 1.25). Digital images were color balanced with Adobe Photoshop 8.0 (Adobe Systems, San Jose, CA). The composition of the images was not altered. The intensity profile of Cx43 immunoreactivity as a function of depth in the ONL was performed with the Plot Profile function in ImageJ software (NIH). Three plot profiles corresponding to randomly selected regions of interest, 30μm in width and 200μm in length, oriented with the major axis perpendicular to the inner ONL border were averaged for each image.

Analysis of physiological data

Current amplitudes were measured at the end of applied voltage pulses. Data normalization was done relative to the maximum amplitude measured for each cell in control conditions. To find maxima and minima of conductance across the −140 to 80mV range of membrane potential we fit an 8^{th} degree polynomial function to the I/V curve of each cell and differentiated this function with respect to Vm using Origin software (OriginLab Corp, Northhampton, MA) to calculate the slope conductance. Maxima ($Gmax_i$ and $Gmax_o$) and minima (Gmin) were measured with the data reader function in Origin software. When a minimum in the conductance curve was not obvious (i.e. monotonic decrease or increase with Vm) the conductance values at the extreme membrane potentials (−140 and 80mV) defined $Gmax_i$ and $Gmax_o$, respectively, and the conductance at the average membrane potential where Gmin occurred (−20 mV) defined Gmin. Blocker-sensitive currents were calculated as the subtraction trace by trace of total currents in the presence of the blocker from total current in control conditions, using Clampfit software (Molecular Devices). Percent inhibition produced by channel blockers was calculated as I_b/I_c*100 for the indicated Vm, where I_b is the amplitude of the blocker-sensitive current and I_c is the current in control conditions for the same Vm. To determine the voltage of activation we calculated the chord conductance at each Vm as $G_K = I_s / (Vm-E_K)$, where I_s is the blocker-sensitive current (Ba^{2+} or TEA), Vm is the voltage command and E_K is the estimated reversal potential for K^+ in our conditions ($E_K = −101mV$). The voltage of activation was determined

as the Vm at which the chord conductance was at least 5% of the chord conductance calculated for −140mV or 80mV for the Ba^{2+}-sensitive and the TEA-sensitive current, respectively. The voltage of half-maximal activation (V_{50}) was calculated from a Botzman fit to the normalized curve of chord conductance.

Graphs and statistical analysis

Graphs and statistical analyses were done with Prism 4 (GraphPad, La Jolla, CA). Statistical values are the mean ± standard error of the mean (SEM), with *n* the number of cells tested. Tests used for statistical comparisons are found in the figure legends. Deviation from the mean in 3D was calculated for each cell as $\sqrt{(Gmax_i - \overline{Gmax_i})^2 + (Gmax_o - \overline{Gmax_o})^2 + (Gmin - \overline{Gmin})^2}$ where $Gmax_i$, $Gmax_o$ and *Gmin* are maxima and minima of conductance across the −140 to 80mV range and $\overline{Gmaxi}$, $\overline{Gmin}$ and $\overline{Gmaxo}$ are average values.

Results

Variability of OEC membrane conductance

We previously showed that gap junction coupled OECs display low input resistance (R_i) and an ohmic behavior across a wide range of membrane potentials. In contrast, uncoupled OECs display high R_i and voltage-dependent conductances revealed by the departure from ohmic behavior in the current vs. voltage (I/V) curve (Rela et al. 2010). However, the mechanisms explaining departure from linearity were unknown. Here we developed a sensitive analysis to quantify OEC departure from linearity in the I/V curve. The analysis is based on detecting changes in the macroscopic slope conductance as a function of Vm, that is, in the derivative of the I/V curve. Linear I/V curves are expected to produce a fairly constant conductance function while nonlinear I/V curves generate a function with extreme values (minima and/or maxima) at specific Vm values, depending on the voltage-dependent conductances recruited at specific voltage ranges. Figure 1A1 shows an OEC with high R_i and a nonlinear I/V curve. The conductance function derived from the I/V curve displays a minimum of conductance (Gmin) near −50 mV (Figure 1A2). A hyperpolarization-activated inward current produces a maximum conductance ($Gmax_i$) near −100 mV while a depolarization-activated outward current produces a maximum conductance ($Gmax_o$) near 0 mV. In contrast, the maxima and minimum of conductance were less pronounced in OECs with low R_i and a highly linear I/V curve, typical of gap junction coupled cells (Rela et al. 2010). Consistent with a lower R_i, the conductance was higher in linear cells across the voltage range analyzed. Between these two extremes, variability in OECs is observed in the membrane conductances and the degree of nonlinearity. $Gmax_i$, Gmin and $Gmax_o$ did not have normal distributions whereas V_r values were normally distributed, showed little variation (−79 ± 1 mV, n=56) and were in the range expected for glial cells (Figure 1B). Despite variability, $Gmax_i$ and $Gmax_o$ were significantly higher than Gmin, indicating that the nonlinearity of the I/V curve is a salient characteristic of OECs (Figure 1C). This suggests that voltage-activated conductances are variably expressed in OECs.

Different voltage-activated K^+ conductances shape OEC I/V profiles

To evaluate whether voltage-activated currents producing nonlinearities in the I/V curve of OECs were mediated by K^+ channels we tested their sensitivity to K^+ channel blockers. Figure 2A1 is typical of the Ba^{2+} block of a hyperpolarization-activated inward component of the total current that resulted in a reduction of $Gmax_i$ (Figure 2A2). The Ba^{2+}-sensitive component showed a marked inward rectification, activated at membrane potentials more negative than 0 mV in average, had a V_{50} of −60 ± 12 mV, reversed at −90 ± 10 mV, and represented 61 ± 1% of the inward current measured at −140 mV (Figure 2B,C). This Ba^{2+} concentration effectively blocks many inward rectifier K^+ channels (K_{ir}) and is largely ineffective on delayed rectifier K^+ channels (K_{DR}) (Coetzee et al. 1999; IUPHAR 2005; Klumpp et al. 1995). The hyperpolarization-activated inward current was also sensitive to 3 mM Cs^+ (n=2, Figure S1). Conversely, TEA (20 mM), a blocker of K^+ channels, blocked a depolarization-activated outward component of the total current (Figure 3A1), resulting in a reduction of $Gmax_o$ (Figure 3A2). The TEA-sensitive component showed outward rectification, had a delayed activation at membrane potentials more positive than 0 mV in average, a V_{50} of 9 ± 14 mV and represented 41 ± 1% of the outward current when measured at 80 mV (Figure 3B,C). These results show that OECs display at least two pharmacologically distinct K^+ membrane currents: 1) Ba^{2+}-sensitive hyperpolarization-activated inward current, compatible with K_{ir} channels; and 2) TEA-sensitive depolarization-activated outward current, compatible with K^+ channels of the delayed rectifier type (K_{DR}).

To test whether this analysis could detect variations in the I/V curve of coupled OECs, it was applied to OECs treated with a gap junction blocker, meclofenamic acid (MFA), which increases the R_i and the nonlinearity of the I/V curve of OECs (Rela et al. 2010). Figure 4A1 shows a representative example, in which MFA (100 μM) blocked a component of the total current across the voltage range analyzed, resulting in a larger reduction of Gmin compared to $Gmax_i$, and $Gmax_o$, exacerbating the nonlinearity of the I/V curve (Figure 4A2). The MFA-sensitive component showed an ohmic behavior as indicated by a good linear fit to the I/V curve (r^2=0.982) and reversed close to −70 mV near the OEC average V_r, as expected for nonspecific currents mediated by gap junctions. The MFA-sensitive current represented 64 ± 06 % of the inward current when measured at −140 mV and 52 ± 07% of the outward current when measured at 80 mV (Figure 4B,C, not significantly different, Wilcoxon test). These results indicate that $Gmax_i$, Gmin and $Gmax_o$ reliably monitor changes in conductance across the −140 to 80 mV range of membrane potential in OECs and are useful to detect the recruitment of hyperpolarization- or depolarization-activated conductances.

Ba^{2+} produced a significant reduction of $Gmax_i$ and membrane depolarization, indicating a Ba^{2+}-sensitive inwardly rectifying conductance active at rest (Figure 5A). Conversely, TEA resulted in a significant reduction of $Gmax_o$ with no change in V_r, $Gmax_i$ or Gmin (Figure 5B). Finally, MFA produced a significant reduction of $Gmax_i$ and Gmin and a significant hyperpolarization (Figure 5C). These results indicate that K_{ir} channels and gap junctions are principal contributors to the whole cell conductance near the V_r and that K_{DR} channels and gap junctions contribute to the whole cell conductance in depolarized OECs.

To address voltage-activated K^+ channels contributions to the nonlinearity of OEC I/V curve, we analyzed the effect of channel blockers on the salience of differences in conductance across the −140 to 80 mV voltage range: we compared $Gmax_i$ and $Gmax_o$ to Gmin in control conditions versus each of the blockers. A significant difference between Gmax –either in the inward or the outward direction- and Gmin was taken as evidence of a salient nonlinearity of the I/V curve in the corresponding voltage range. Ba^{2+} eliminated the significant difference between $Gmax_i$ and Gmin present in control conditions, while a significant difference between $Gmax_o$ and Gmin was not affected by Ba^{2+} (Figure 5A1). TEA eliminated a significant difference between $Gmax_o$ and Gmin present in control conditions, while a significant difference between $Gmax_i$ and Gmin was not affected by TEA (Figure 5B1). MFA, which unmasks voltage dependent conductances of OECs by blocking the large linear gap junction conductance, increased the nonlinearity of the I/V curve. This was seen as a significant difference between $Gmax_o$ and Gmin that appeared with MFA and was absent in control conditions (Figure 5C1). Sensitivity to Ba^{2+} and TEA was preserved after MFA-sensitive currents were blocked (Figure S2). Collectively, these results show that K_{ir} and K_{DR} channels contribute to the nonlinear behavior of the I/V curve of OECs at hyperpolarized or depolarized membrane potentials, respectively, and that gap junction coupling can mask this contribution with the recording configuration that we used.

In light of these results, and because R_i is determined around rest it becomes clear that R_i values are mostly determined by K_{ir} and gap junction conductance. R_i values in OECs fit a bimodal function (Figure 5D), suggesting at least two populations of OECs that differ in gap junction expression and/or K_{ir} conductance. This is supported by previous data indicating that cells with high R_i are insensitive to MFA (Rela et al. 2010). Because Gmin was only affected by MFA (Figure 5) it is a useful parameter to isolate and characterize gap junction connectivity of OECs. Finally, the analysis of conductance proved more sensitive to pharmacologically identify voltage activated conductances in OECs compared to direct measurements of current amplitudes, which escaped the detection of Ba^{2+} sensitivity (Figure S3).

I/V profiles of OECs were not significantly affected by the application of a 200-msec preconditioning pulse to either −160 mV or −40 mV before the series of test voltage steps, indicating the lack of transient K^+ currents of the A-type in OECs (n=7, Figure S4A). Fast voltage-activated inward currents -likely sodium currents- were observed in only 2/56 cells in control conditions and the average current amplitude elicited by a voltage step to −20 mV from a holding potential of −80 mV was 210 pA (Figure S4B–C). Fast inward currents were not observed in the presence of MFA (Figure S4D), suggesting that gap junctions were not masking the expression of sodium currents.

Contribution of K^+ channels to variability

Because the OEC population displayed a large variability in membrane conductance and in the linearity of the I/V curve in control conditions, the question arises whether the effect of channel blockers is differentially dependent on the initial membrane properties. To address this we performed linear regression analyses between the change in conductance caused by each blocker and the control conductance when significant effects found when comparing

control versus blocker (Figure 6A). Higher reductions of $Gmax_i$ produced by Ba^{2+} corresponded to higher initial $Gmax_i$ values (Figure 6B1), higher reductions of $Gmax_o$ produced by TEA corresponded to higher initial $Gmax_o$ values (Figure 6B2) and higher reductions of $Gmax_i$ and Gmin caused by MFA corresponded to higher initial $Gmax_i$ and Gmin values, respectively (Figure 6B3). These results confirmed that variability in the amplitude of the Ba^{2+}-sensitive and the TEA-sensitive conductances partially accounted for the variability in the whole cell conductance at hyperpolarized and depolarized potentials, respectively.

These results suggest that variability in K^+ channel expression and in gap junction coupling contribute to the heterogeneity of OEC biophysical properties. To further quantify the contributions of each conductance, we characterized the variability of membrane conductance across the range of Vm studied in the OECs that were exposed to each blocker. We calculated the distance to the mean value of conductance for each OEC in 3D representations of $Gmax_i$, Gmin and $Gmax_o$ (see Figure S5), before and after treatment for each channel blocker (Figure 7A1) and used these data as informative of the variability of membrane conductance in OECs. Figure 7A2 shows that all blockers produced a significant reduction in variability; however, there were no significant differences among the different blockers, suggesting that K_{ir} channels, K_{DR} channels and gap junction channels contributed comparably to variability.

A high degree of gap junction coupling could interfere with the recruitment of voltage dependent K^+ conductances owing to a shunting effect. To test this idea we evaluated whether the sensitivity to K^+ channel blockers correlated with an estimate of the gap junction conductance before treatment. The gap junction conductance was constant across the entire voltage range as indicated by the linearity of the I/V curve of MFA-sensitive currents (Figure 4C) and as Gmin was sensitive only to MFA we considered it an informative estimate of the gap junction conductance. Figure 7B1 shows that sensitivity to Ba^{2+} decreased as Gmin increased with the two variables showing a strong negative correlation. In contrast, the sensitivity to TEA did not correlate with Gmin (Figure 7B2). These results suggest that K_{ir} channels are more susceptible to shunting effects of gap junctions than K_{DR} channels. Alternatively, K_{ir} channels may be structurally and/or functionally dependent on gap junctions.

Variability in OEC molecular phenotype and responsiveness to OSN activity is associated with depth in the ONL (Au et al. 2002; Thyssen et al. 2013). Consequently, we asked whether the sensitivity to channel blockers was spatially organized through the ONL. We analyzed to determine if there is a correlation between the sensitivity to each blocker with the depth of recorded cells in the ONL, considering deeper cells those closer to the glomerular layer and more superficial cells those closer to the OB surface. Sensitivity to K^+ channel blockers did not correlate with OEC depth in the ONL. However, deep OECs were more susceptible to the gap junction blocker MFA than superficial OECs (Figure 8A). In accord, connexin 43 (Cx43) -the most likely candidate mediating OEC gap junction coupling- labeling was higher in the deep ONL and gradually decreased towards the OB surface (Figure 8B) (Rela et al. 2010). The molecular identification of K^+ channels was not pursued here; however, we tested whether the main K_{ir} subunit expressed by astrocytes and

Müller glia ($K_{ir}4.1$) was present in OECs. $K_{ir}4.1$ immunoreactivity was scarce in the ONL and did not colocalize with S100B, a marker of OECs (Figure S6) suggesting that this subunit is not the molecular substrate for K_{ir} currents of OECs.

Discussion

There is a consensus that glial cells are highly permeable to K^+ and have V_r near the equilibrium potential for K^+. Differences in the types of K^+ channels have been reported in different glial types, areas of the brain, maturational states and in pathological vs. normal conditions (Baker 2002; Kofuji and Newman 2004; Olsen and Sontheimer 2008). Importantly, the repertoire of K^+ channels can differ when comparing cultured or acutely isolated glial cells with those recorded in conditions that preserve tissue structure (Bordey and Sontheimer 2000; Nashmi et al. 2002). Here we show that OECs recorded from acute slices of the OB displayed at least two different K^+ conductances: 1) A hyperpolarization-activated Ba^{2+}-sensitive inward current compatible with K_{ir} channels; and 2) A depolarization-activated TEA-sensitive outward current compatible with K_{DR} channels. We previously showed that the voltage-dependent outward current contributes to the nonlinearity of the I-V curve and can be masked by gap junction coupling (Rela et al. 2010). Depolarization-activated chloride channels have been described in Schwann cells (Ritchie 1987). Considering that in our recording conditions the reversal potential for chloride is close to 0 mV, we cannot rule out the possibility that the TEA-insensitive component of the depolarization-activated outward current is carried by chloride ions instead of reflecting a gap junction conductance.

Possible roles of K^+ channels in OECs

K_{ir} channels are implicated in the maintenance of the negative V_r typical of glial cells and in the homeostasis of the extracellular concentration of K^+, i.e. K^+ buffering (Bay and Butt 2012; Kofuji et al. 2000; Kucheryavykh et al. 2007; Olsen et al. 2006). Impaired K^+ buffering and a higher probability of epileptiform activity is observed in glial cells with deficient expression of gap junction channels, suggesting that gap junctions act together with K_{ir} channels to buffer K^+ in the extracellular space (Menichella et al. 2006; Wallraff et al. 2006). Our data show that OECs express both K_{ir} and gap junction channels that may support K^+ buffering in the olfactory nerve. Because K_{ir} channels play a major role in maintaining a hyperpolarized potential, they are also essential for glial functions that depend on a hyperpolarized membrane potential, like glutamate uptake (Djukic et al. 2007; Kucheryavykh et al. 2007). OECs respond to glutamate (Rieger et al. 2007; Thyssen et al. 2010), and it is possible that K^+ channels are involved in glutamate uptake by OECs.

Based on previous reports (Higashi et al. 2001) and data in Figure S6, OEC K_{ir} channels are unlikely constituted by Kir4.1, the most common subunit expressed by astrocytes and oligodendrocytes (Neusch et al. 2001; Poopalasundaram et al. 2000) or $K_{ir}2.1$ subunits, which are expressed by Müller glia together with $K_{ir}4.1$ (Kofuji et al. 2002). Another possible candidate is Kir6.1, a subunit that is expressed by oligodendrocytes and confers ATP sensitivity to the channel (Ammälä et al. 1996). This property remains to be determined for K_{ir} channels in OECs.

K_{DR} channels are implicated in regulation of the cell cycle in astrocytes (MacFarlane and Sontheimer 2000), Schwann cells (Chiu and Wilson 1989) and oligodendrocyte progenitors (Gallo et al. 1996; Vautier et al. 2004). Given that OEC transplants to sites of injury are a candidate strategy to promote regeneration in the CNS, a substantial effort has been made to establish which growth factors promote OEC proliferation in culture with the goal of obtaining significant numbers of OECs for transplant (Chuah and Teague 1999; Vukovic et al. 2009; Wang et al. 2012; Yan et al. 2001). There is evidence that at least two growth factors that promote proliferation in OECs -platelet-derived growth factor (PDGF) and insulin-like growth factor 1 (IGF-1)- also promote proliferation in other cell types, an effect that involves the participation of K_{DR} channels (Gallo et al. 1996; Pappas and Ritchie 1998; Sobko et al. 1998). OECs proliferate *in vivo* and proliferation can be upregulated after bulbectomy, however, the mechanisms remain unknown (Chehrehasa et al. 2012; Watanabe et al. 2006).

We did not find transient A-type K^+ currents in OECs. The role of A-type K^+ currents in glia is not clear. Rapidly inactivating K^+ currents of the A-type upregulate in response to ischemic injury and inflammation in Müller glial cells, (Pannicke et al. 2005a; Pannicke et al. 2005b), a retinal glial cell regarded as similar to OECs in terms of plasticity and molecular phenotype (Gudiño-Cabrera and Nieto-Sampedro 1999). Whether OECs upregulate A-type K^+ channels under pathological conditions -and its physiological significance- remains to be established. Finally, A-type K^+ currents are developmentally down-regulated in hippocampal astrocytes (Kressin et al. 1995) and Müller glia (Bringmann et al. 1999) and we cannot rule out the expression of A-type K^+ currents in OECs from animals younger than those used in our study.

The gap junction channel blocker MFA produced a slight hyperpolarization of OECs. This was surprising for a selective block of gap junctions, since electrically coupled OECs are expected to be equipotential. However, our results suggest that gap junctions exert a shunting effect on K_{ir} channels (Figure 7). As K_{ir} channels determine in part the resting potential (Figure 5), if a shunting effect on K_{ir} channels is removed by the gap junction blocker MFA, a bigger impact of the K_{ir} conductance on the resting potential is expected, leading to hyperpolarization. Alternatively, activation of KCNQ potassium channels and concomitant hyperpolarization by MFA were reported in cultured neurons (Peretz et al. 2005). KCNQ channels are functionally expressed in oligodendrocyte precursors (Wang et al. 2011) and could underlie the hyperpolarizing effect of MFA in OECs. Considering that the net effect of MFA is a general reduction of the whole cell current across a wide range of Vm and that our previous work showed the abolishment of coupling currents by MFA in double recordings of OECs (Rela et al. 2010), the dominant effect of MFA on OEC electrophysiological properties is the block of gap junctions and thus their potential shunting effects.

Heterogeneity of OECs

Olfactory bulb OECs are a heterogeneous population of cells in terms of biochemical markers. The expression of glial fibrillary acidic protein (GFAP) is more prominent in OECs localized in the most superficial portion of the olfactory nerve layer of the OB (outer ONL)

and neuropeptide Y (NPY) is more prominently expressed by OECs in the inner ONL (Au et al. 2002). OECs can also be distinguished in terms of expression levels of the low-affinity nerve growth factor receptor p75. OECs expressing high levels of p75 are biased towards the expression of genes that participate in extracellular matrix modulation and OECs expressing low levels of p75 are biased towards the expression of genes involved in axon guidance (Honoré et al. 2012). Physiologically, outer OECs respond to glutamate -the main neurotransmitter released by OSNs- with transient elevations of intracellular calcium, while inner OECs do not (Thyssen et al. 2013). The heterogeneity observed in OEC biophysical properties is additional evidence of OECs subpopulations. Our data show that OECs with an electrophysiological signature characterized by large, ohmic membrane conductance are integrated to a glial network equipped for efficient potassium buffering (i.e. large gap junction and K_{ir} conductance). This signature is more prominent in inner OECs. Conversely, OECs characterized by a salient voltage-dependent membrane conductance are rare, isolated from the glial network and electrophysiologically compatible with a proliferative state (i.e. small gap junction and salient K_{DR} conductance) (Fieber et al. 2003; Gallo et al. 1996; Pappas and Ritchie 1998; Sobko et al. 1998). The higher immunoreactivity for Cx43 in the inner ONL strengthens the idea that it mediates gap junction coupling in OECs. The significance of this heterogeneity is not known, however, it may arise from developmental processes (Forni et al. 2011) or OECs in different stages of the cell cycle or differentiation. The axons associated with OECs differ in their maturation due to the ongoing turnover of the olfactory sensory neurons. Consequently, the heterogeneity observed in OECs may be explained by variability in the signals coming from axons during growth or with stability following synapse formation (Rieger et al. 2007; Thyssen et al. 2013). Finally, heterogeneity may arise from an interaction between the architecture of the cells recorded, the location of the channels and the location of the recording site (Rela et al. 2010). It will be interesting to use computer modeling to analyze possible interactions between the location of gap junction coupling sites and heterogeneity in the distribution of voltage-dependent channels. One plausible scenario is that gap junctions have shunting effects regulating the activation of voltage-dependent channels, a possibility supported by our data for the case of K_{ir} channels.

OECs as specialized astrocyte-like cells

OECs *in vivo* have a unique non-myelinating mesh-like morphology and a molecular profile that distinguishes them from other glial types. For example, OECs highly express S100B, also expressed by immature and mature astrocyte and oligodendrocyte lineages (Hachem et al. 2005; Rela et al. 2010), PLP, typical of myelinating glia (Griffiths et al. 1995; Puckett et al. 1987), and BLBP, also expressed by radial and Bergmann glia, associated with neuron migration, and by neural stem cells (Feng et al. 1994; Platel et al. 2009; Rela et al. 2010).

We previously showed that OECs display a gap junction coupling similar to that of astrocytes. In astrocytes gap junctions contain both Cx43 and connexin 30 (Cx30). OECs, however, express Cx43 as the main gap junction constituent, and do not express Cx30 (Rela et al. 2010). Here we show that OECs express diverse K^+ membrane currents also displayed by other glial types. If we consider only data obtained from preparations that preserve tissue structure, OECs share similarities with astrocytes in terms of gap junction coupling, and K_{ir} channels, however, the main molecules underlying the currents may differ. In addition,

OECs lack the inactivating A-type K^+ currents characteristic of astrocytes (Bordey and Sontheimer 1997). Further, the voltage-activated sodium currents found in cerebellar Bergmann glia (Bordey and Sontheimer 2000) and Schwann cells associated with unmyelinated axons (Chiu 1988) are not typical of OECs. K^+ currents of OECs resemble the profiles observed for mature oligodendrocytes (Gipson and Bordey 2002), but the connexins mediating gap junction coupling differ (Maglione et al. 2010). Our data is restricted to OECs in the OB and whether OECs from the lamina propria of the olfactory epithelium or from the peripheral segments of the olfactory nerve share the same properties remains to be determined.

These data contribute to our understanding of the physiology of OECs *in situ*, where their axon promoting properties appear optimal. Understanding the relevance of these properties for axon growth and how to maintain them *ex vivo* and following transplantation is of utmost importance for those considering OECs as a therapeutic strategy for CNS repair.

Supplementary Material

Refer to Web version on PubMed Central for supplementary material.

Acknowledgements

This work was supported by NIH (DC007880, DC006972, DC000210, DC012441) and Secretaría de Ciencia, Tecnología e Innovación Productiva (PICT2011-1650), Universidad de Buenos Aires (UBACYT 20020100100562), and Consejo Nacional de Investigaciones Científicas y Técnicas, Argentina. We are grateful to Drs. M. Rafael Pagani and Valeria Della Maggiore, and all members of the Greer laboratory for invaluable discussions and critical reading of the manuscript. We thank Dr. Jorge Colombo (CEMIC, Buenos Aires, Argentina), for providing the Kir4.1 antibody.

References

Akiyama Y, Lankford K, Radtke C, Greer CA, Kocsis JD. Remyelination of spinal cord axons by olfactory ensheathing cells and Schwann cells derived from a transgenic rat expressing alkaline phosphatase marker gene. Neuron Glia Biol. 2004; 1(1):47–55. [PubMed: 16799702]

Alexander CL, Fitzgerald UF, Barnett SC. Identification of growth factors that promote long-term proliferation of olfactory ensheathing cells and modulate their antigenic phenotype. Glia. 2002; 37(4):349–364. [PubMed: 11870874]

Ammälä C, Moorhouse A, Ashcroft FM. The sulphonylurea receptor confers diazoxide sensitivity on the inwardly rectifying K+ channel Kir6.1 expressed in human embryonic kidney cells. J Physiol. 1996; 494(pt 3):709–714. [PubMed: 8865068]

Au WW, Treloar HB, Greer CA. Sublaminar organization of the mouse olfactory bulb nerve layer. J Comp Neurol. 2002; 446(1):68–80. [PubMed: 11920721]

Baker MD. Electrophysiology of mammalian Schwann cells. Prog Biophys Mol Biol. 2002; 78(2–3): 83–103. [PubMed: 12429109]

Bartolomei JC, Greer CA. Olfactory ensheathing cells: bridging the gap in spinal cord injury. Neurosurgery. 2000; 47(5):1057–1069. [PubMed: 11063098]

Bay V, Butt AM. Relationship between glial potassium regulation and axon excitability: a role for glial Kir4.1 channels. Glia. 2012; 60(4):651–660. [PubMed: 22290828]

Bordey A, Sontheimer H. Postnatal development of ionic currents in rat hippocampal astrocytes in situ. J Neurophysiol. 1997; 78(1):461–477. [PubMed: 9242294]

Bordey A, Sontheimer H. Ion channel expression by astrocytes in situ: comparison of different CNS regions. Glia. 2000; 30(1):27–38. [PubMed: 10696142]

Bringmann A, Biedermann B, Reichenbach A. Expression of potassium channels during postnatal differentiation of rabbit Müller glial cells. Eur J Neurosci. 1999; 11(8):2883–2896. [PubMed: 10457185]

Caggiano M, Kauer JS, Hunter DD. Globose basal cells are neuronal progenitors in the olfactory epithelium: a lineage analysis using a replication-incompetent retrovirus. Neuron. 1994; 13(2): 339–352. [PubMed: 8060615]

Chehrehasa F, Ekberg JA, Lineburg K, Amaya D, Mackay-Sim A, St John JA. Two phases of replacement replenish the olfactory ensheathing cell population after injury in postnatal mice. Glia. 2012; 60(2):322–332. [PubMed: 22065423]

Chiu SY. Changes in excitable membrane properties in Schwann cells of adult rabbit sciatic nerves following nerve transection. J Physiol. 1988; 396:173–188. [PubMed: 2457688]

Chiu SY, Wilson GF. The role of potassium channels in Schwann cell proliferation in Wallerian degeneration of explant rabbit sciatic nerves. J Physiol. 1989; 408:199–222. [PubMed: 2476555]

Chuah MI, Teague R. Basic fibroblast growth factor in the primary olfactory pathway: mitogenic effect on ensheathing cells. Neuroscience. 1999; 88(4):1043–1050. [PubMed: 10336119]

Coetzee WA, Amarillo Y, Chiu J, Chow A, Lau D, McCormack T, Moreno H, Nadal MS, Ozaita A, Pountney D, et al. Molecular diversity of K+ channels. Ann N Y Acad Sci. 1999; 868:233–285. [PubMed: 10414301]

Djukic B, Casper KB, Philpot BD, Chin LS, McCarthy KD. Conditional knock-out of Kir4.1 leads to glial membrane depolarization, inhibition of potassium and glutamate uptake, and enhanced short-term synaptic potentiation. J Neurosci. 2007; 27(42):11354–11365. [PubMed: 17942730]

Dlouhy BJ, Awe O, Rao RC, Kirby PA, Hitchon PW. Autograft-derived spinal cord mass following olfactory mucosal cell transplantation in a spinal cord injury patient: Case report. J Neurosurg Spine. 2014; 21(4):618–622. [PubMed: 25002238]

Dobkin BH, Curt A, Guest J. Cellular transplants in China: observational study from the largest human experiment in chronic spinal cord injury. Neurorehabil Neural Repair. 2006; 20(1):5–13. [PubMed: 16467274]

Doucette R. Glial influences on axonal growth in the primary olfactory system. Glia. 1990; 3(6):433–449. [PubMed: 2148546]

Doucette R. PNS-CNS transitional zone of the first cranial nerve. J Comp Neurol. 1991; 312(3):451–466. [PubMed: 1748741]

Dunning MD, Lakatos A, Loizou L, Kettunen M, ffrench-Constant C, Brindle KM, Franklin RJ. Superparamagnetic iron oxide-labeled Schwann cells and olfactory ensheathing cells can be traced in vivo by magnetic resonance imaging and retain functional properties after transplantation into the CNS. J Neurosci. 2004; 24(44):9799–9810. [PubMed: 15525765]

Feng L, Hatten ME, Heintz N. Brain lipid-binding protein (BLBP): a novel signaling system in the developing mammalian CNS. Neuron. 1994; 12(4):895–908. [PubMed: 8161459]

Feron F, Perry C, Cochrane J, Licina P, Nowitzke A, Urquhart S, Geraghty T, Mackay-Sim A. Autologous olfactory ensheathing cell transplantation in human spinal cord injury. Brain. 2005; 128(Pt 12):2951–2960. [PubMed: 16219671]

Fieber LA, González DM, Wallace MR, Muir D. Delayed rectifier K currents in NF1 Schwann cells. Pharmacological block inhibits proliferation. Neurobiol Dis. 2003; 13(2):136–146. [PubMed: 12828937]

Forni PE, Taylor-Burds C, Melvin VS, Williams T, Wray S. Neural crest and ectodermal cells intermix in the nasal placode to give rise to GnRH-1 neurons, sensory neurons, and olfactory ensheathing cells. J Neurosci. 2011; 31(18):6915–6927. [PubMed: 21543621]

Franceschini IA, Barnett SC. Low-affinity NGF-receptor and E-N-CAM expression define two types of olfactory nerve ensheathing cells that share a common lineage. Dev Biol. 1996; 173(1):327–343. [PubMed: 8575633]

Gallo V, Zhou JM, McBain CJ, Wright P, Knutson PL, Armstrong RC. Oligodendrocyte progenitor cell proliferation and lineage progression are regulated by glutamate receptor-mediated K+ channel block. J Neurosci. 1996; 16(8):2659–2670. [PubMed: 8786442]

Gipson K, Bordey A. Analysis of the K+ current profile of mature rat oligodendrocytes in situ. J Membr Biol. 2002; 189(3):201–212. [PubMed: 12395285]

Gogos J, Osborne J, Nemes A, Mendelsohn M, Axel R. Genetic ablation and restoration of the olfactory topographic map. Cell. 2000; 103(4):609–620. [PubMed: 11106731]

Graziadei PP, Graziadei GA. Neurogenesis and neuron regeneration in the olfactory system of mammals. I. Morphological aspects of differentiation and structural organization of the olfactory sensory neurons. J Neurocytol. 1979; 8(1):1–18. [PubMed: 438867]

Griffiths IR, Dickinson P, Montague P. Expression of the proteolipid protein gene in glial cells of the post-natal peripheral nervous system of rodents. Neuropathol Appl Neurobiol. 1995; 21(2):97–110. [PubMed: 7541902]

Gudiño-Cabrera G, Nieto-Sampedro M. Estrogen receptor immunoreactivity in Schwann-like brain macroglia. J Neurobiol. 1999; 40(4):458–470. [PubMed: 10453049]

Hachem S, Aguirre A, Vives V, Marks A, Gallo V, Legraverend C. Spatial and temporal expression of S100B in cells of oligodendrocyte lineage. Glia. 2005; 51(2):81–97. [PubMed: 15782413]

Harding JW, Wright JW. Reversible effects of olfactory nerve section on behavior and biochemistry in mice. Brain Res Bull. 1979; 4(1):17–22. [PubMed: 89004]

Harrop JS, Hashimoto R, Norvell D, Raich A, Aarabi B, Grossman RG, Guest JD, Tator CH, Chapman J, Fehlings MG. Evaluation of clinical experience using cell-based therapies in patients with spinal cord injury: a systematic review. J Neurosurg Spine. 2012; 17(1 Suppl):230–246. [PubMed: 22985383]

Hayat S, Wigley C, Robbins J. Intracellular calcium handling in rat olfactory ensheathing cells and its role in axonal regeneration. Mol Cell Neurosci. 2003; 22(2):259–270. [PubMed: 12676535]

Higashi K, Fujita A, Inanobe A, Tanemoto M, Doi K, Kubo T, Kurachi Y. An inwardly rectifying K(+) channel, Kir4.1, expressed in astrocytes surrounds synapses and blood vessels in brain. Am J Physiol Cell Physiol. 2001; 281(3):C922–C931. [PubMed: 11502569]

Honoré A, Le Corre S, Derambure C, Normand R, Duclos C, Boyer O, Marie JP, Guérout N. Isolation, characterization, and genetic profiling of subpopulations of olfactory ensheathing cells from the olfactory bulb. Glia. 2012; 60(3):404–413. [PubMed: 22161947]

Huang H, Chen L, Wang H, Xiu B, Li B, Wang R, Zhang J, Zhang F, Gu Z, Li Y, et al. Influence of patients' age on functional recovery after transplantation of olfactory ensheathing cells into injured spinal cord injury. Chin Med J (Engl). 2003; 116(10):1488–1491. [PubMed: 14570607]

IUPHAR. Compendium of Voltage-Gated Ion Channels. 2005

Kafitz KW, Greer CA. Differential expression of extracellular matrix and cell adhesion molecules in the olfactory nerve and glomerular layers of adult rats. J Neurobiol. 1998; 34(3):271–282. [PubMed: 9485051]

Kafitz KW, Greer CA. Olfactory ensheathing cells promote neurite extension from embryonic olfactory receptor cells in vitro. Glia. 1999; 25(2):99–110. [PubMed: 9890625]

Klumpp DJ, Song EJ, Ito S, Sheng MH, Jan LY, Pinto LH. The Shaker-like potassium channels of the mouse rod bipolar cell and their contributions to the membrane current. J Neurosci. 1995; 15(7 Pt 1):5004–5013. [PubMed: 7623129]

Kofuji P, Biedermann B, Siddharthan V, Raap M, Iandiev I, Milenkovic I, Thomzig A, Veh RW, Bringmann A, Reichenbach A. Kir potassium channel subunit expression in retinal glial cells: implications for spatial potassium buffering. Glia. 2002; 39(3):292–303. [PubMed: 12203395]

Kofuji P, Ceelen P, Zahs KR, Surbeck LW, Lester HA, Newman EA. Genetic inactivation of an inwardly rectifying potassium channel (Kir4.1 subunit) in mice: phenotypic impact in retina. J Neurosci. 2000; 20(15):5733–5740. [PubMed: 10908613]

Kofuji P, Newman EA. Potassium buffering in the central nervous system. Neuroscience. 2004; 129(4):1045–1056. [PubMed: 15561419]

Kressin K, Kuprijanova E, Jabs R, Seifert G, Steinhäuser C. Developmental regulation of Na+ and K+ conductances in glial cells of mouse hippocampal brain slices. Glia. 1995; 15(2):173–187. [PubMed: 8567069]

Kucheryavykh YV, Kucheryavykh LY, Nichols CG, Maldonado HM, Baksi K, Reichenbach A, Skatchkov SN, Eaton MJ. Downregulation of Kir4.1 inward rectifying potassium channel subunits by RNAi impairs potassium transfer and glutamate uptake by cultured cortical astrocytes. Glia. 2007; 55(3):274–281. [PubMed: 17091490]

Liesi P. Laminin-immunoreactive glia distinguish regenerative adult CNS systems from non-regenerative ones. EMBO J. 1985; 4(10):2505–2511. [PubMed: 3902469]

Lima C, Pratas-Vital J, Escada P, Hasse-Ferreira A, Capucho C, Peduzzi JD. Olfactory mucosa autografts in human spinal cord injury: a pilot clinical study. J Spinal Cord Med. 2006; 29(3):191–203. discussion 204-6. [PubMed: 16859223]

MacFarlane SN, Sontheimer H. Changes in ion channel expression accompany cell cycle progression of spinal cord astrocytes. Glia. 2000; 30(1):39–48. [PubMed: 10696143]

Mackay-Sim A, Féron F, Cochrane J, Bassingthwaighte L, Bayliss C, Davies W, Fronek P, Gray C, Kerr G, Licina P, et al. Autologous olfactory ensheathing cell transplantation in human paraplegia: a 3-year clinical trial. Brain. 2008; 131(Pt 9):2376–2386. [PubMed: 18689435]

Maglione M, Tress O, Haas B, Karram K, Trotter J, Willecke K, Kettenmann H. Oligodendrocytes in mouse corpus callosum are coupled via gap junction channels formed by connexin47 and connexin32. Glia. 2010; 58(9):1104–1117. [PubMed: 20468052]

Menichella DM, Majdan M, Awatramani R, Goodenough DA, Sirkowski E, Scherer SS, Paul DL. Genetic and physiological evidence that oligodendrocyte gap junctions contribute to spatial buffering of potassium released during neuronal activity. J Neurosci. 2006; 26(43):10984–10991. [PubMed: 17065440]

Miragall F, Kadmon G, Husmann M, Schachner M. Expression of cell adhesion molecules in the olfactory system of the adult mouse: presence of the embryonic form of N-CAM. Dev Biol. 1988; 129(2):516–531. [PubMed: 3417050]

Nashmi R, Velumian AA, Chung I, Zhang L, Agrawal SK, Fehlings MG. Patch-clamp recordings from white matter glia in thin longitudinal slices of adult rat spinal cord. J Neurosci Methods. 2002; 117(2):159–166. [PubMed: 12100981]

Neusch C, Rozengurt N, Jacobs RE, Lester HA, Kofuji P. Kir4.1 potassium channel subunit is crucial for oligodendrocyte development and in vivo myelination. J Neurosci. 2001; 21(15):5429–5438. [PubMed: 11466414]

Olsen ML, Higashimori H, Campbell SL, Hablitz JJ, Sontheimer H. Functional expression of Kir4.1 channels in spinal cord astrocytes. Glia. 2006; 53(5):516–528. [PubMed: 16369934]

Olsen ML, Sontheimer H. Functional implications for Kir4.1 channels in glial biology: from K+ buffering to cell differentiation. J Neurochem. 2008; 107(3):589–601. [PubMed: 18691387]

Pannicke T, Uckermann O, Iandiev I, Biedermann B, Wiedemann P, Perlman I, Reichenbach A, Bringmann A. Altered membrane physiology in Müller glial cells after transient ischemia of the rat retina. Glia. 2005a; 50(1):1–11. [PubMed: 15593100]

Pannicke T, Uckermann O, Iandiev I, Wiedemann P, Reichenbach A, Bringmann A. Ocular inflammation alters swelling and membrane characteristics of rat Müller glial cells. J Neuroimmunol. 2005b; 161(1–2):145–154. [PubMed: 15748953]

Pappas CA, Ritchie JM. Effect of specific ion channel blockers on cultured Schwann cell proliferation. Glia. 1998; 22(2):113–120. [PubMed: 9537831]

Peretz A, Degani N, Nachman R, Uziyel Y, Gibor G, Shabat D, Attali B. Meclofenamic acid and diclofenac, novel templates of KCNQ2/Q3 potassium channel openers, depress cortical neuron activity and exhibit anticonvulsant properties. Mol Pharmacol. 2005; 67(4):1053–1066. [PubMed: 15598972]

Platel JC, Gordon V, Heintz T, Bordey A. GFAP-GFP neural progenitors are antigenically homogeneous and anchored in their enclosed mosaic niche. Glia. 2009; 57(1):66–78. [PubMed: 18661547]

Poopalasundaram S, Knott C, Shamotienko OG, Foran PG, Dolly JO, Ghiani CA, Gallo V, Wilkin GP. Glial heterogeneity in expression of the inwardly rectifying K(+) channel, Kir4.1, in adult rat CNS. Glia. 2000; 30(4):362–372. [PubMed: 10797616]

Puckett C, Hudson L, Ono K, Friedrich V, Benecke J, Dubois-Dalcq M, Lazzarini RA. Myelin-specific proteolipid protein is expressed in myelinating Schwann cells but is not incorporated into myelin sheaths. J Neurosci Res. 1987; 18(4):511–518. [PubMed: 2449540]

Raisman G, Barnett SC, Ramón-Cueto A. Repair of central nervous system lesions by transplantation of olfactory ensheathing cells. Handb Clin Neurol. 2012; 109:541–549. [PubMed: 23098735]

Ramakers GJ, Verhaagen J, Oestreicher AB, Margolis FL, van Bergen en Henegouwen PM, Gispen WH. Immunolocalization of B-50 (GAP-43) in the mouse olfactory bulb: predominant presence in preterminal axons. J Neurocytol. 1992; 21(12):853–869. [PubMed: 1469462]

Reinhard E, Meier R, Halfter W, Rovelli G, Monard D. Detection of glia-derived nexin in the olfactory system of the rat. Neuron. 1988; 1(5):387–394. [PubMed: 2483098]

Rela L, Bordey A, Greer CA. Olfactory ensheathing cell membrane properties are shaped by connectivity. Glia. 2010; 58(6):665–678. [PubMed: 19998494]

Rieger A, Deitmer J, Lohr C. Axon-glia communication evokes calcium signaling in olfactory ensheathing cells of the developing olfactory bulb. Glia. 2007; 55(4):352–359. [PubMed: 17136772]

Ritchie JM. Voltage-gated cation and anion channels in mammalian Schwann cells and astrocytes. J Physiol (Paris). 1987; 82(4):248–257. [PubMed: 2460619]

Roet KC, Franssen EH, de Bree FM, Essing AH, Zijlstra SJ, Fagoe ND, Eggink HM, Eggers R, Smit AB, van Kesteren RE, et al. A multilevel screening strategy defines a molecular fingerprint of proregenerative olfactory ensheathing cells and identifies SCARB2, a protein that improves regenerative sprouting of injured sensory spinal axons. J Neurosci. 2013; 33(27):11116–11135. [PubMed: 23825416]

Runyan SA, Phelps PE. Mouse olfactory ensheathing glia enhance axon outgrowth on a myelin substrate in vitro. Exp Neurol. 2009; 216(1):95–104. [PubMed: 19100263]

Schwab ME. Repairing the injured spinal cord. Science. 2002; 295(5557):1029–1031. [PubMed: 11834824]

Sobko A, Peretz A, Shirihai O, Etkin S, Cherepanova V, Dagan D, Attali B. Heteromultimeric delayed-rectifier K+ channels in schwann cells: developmental expression and role in cell proliferation. J Neurosci. 1998; 18(24):10398–10408. [PubMed: 9852577]

Tabakow P, Raisman G, Fortuna W, Czyz M, Huber J, Li D, Szewczyk P, Okurowski S, Miedzybrodzki R, Czapiga B, et al. Functional regeneration of supraspinal connections in a patient with transected spinal cord following transplantation of bulbar olfactory ensheathing cells with peripheral nerve bridging. Cell Transplant. 2014; 23(12):1631–1655. [PubMed: 25338642]

Thyssen A, Hirnet D, Wolburg H, Schmalzing G, Deitmer JW, Lohr C. Ectopic vesicular neurotransmitter release along sensory axons mediates neurovascular coupling via glial calcium signaling. Proc Natl Acad Sci U S A. 2010; 107(34):15258–15263. [PubMed: 20696909]

Thyssen A, Stavermann M, Buddrus K, Doengi M, Ekberg JA, St John JA, Deitmer JW, Lohr C. Spatial and developmental heterogeneity of calcium signaling in olfactory ensheathing cells. Glia. 2013; 61(3):327–337. [PubMed: 23109369]

Tiwari-Woodruff S, Beltran-Parrazal L, Charles A, Keck T, Vu T, Bronstein J. K+ channel KV3.1 associates with OSP/claudin-11 and regulates oligodendrocyte development. Am J Physiol Cell Physiol. 2006; 291(4):C687–C698. [PubMed: 16624990]

Turner CP, Perez-Polo JR. Expression of p75NGFR in the olfactory system following peripheral deafferentation. Neuroreport. 1993; 4(8):1023–1026. [PubMed: 8241456]

Valverde F, Lopez-Mascaraque L. Neuroglial arrangements in the olfactory glomeruli of the hedgehog. J Comp Neurol. 1991; 307(4):658–674. [PubMed: 1714466]

Vautier F, Belachew S, Chittajallu R, Gallo V. Shaker-type potassium channel subunits differentially control oligodendrocyte progenitor proliferation. Glia. 2004; 48(4):337–345. [PubMed: 15390108]

Vincent AJ, West AK, Chuah MI. Morphological plasticity of olfactory ensheathing cells is regulated by cAMP and endothelin-1. Glia. 2003; 41(4):393–403. [PubMed: 12555206]

Vukovic J, Ruitenberg MJ, Roet K, Franssen E, Arulpragasam A, Sasaki T, Verhaagen J, Harvey AR, Busfield SJ, Plant GW. The glycoprotein fibulin-3 regulates morphology and motility of olfactory ensheathing cells in vitro. Glia. 2009; 57(4):424–443. [PubMed: 18803302]

Wallraff A, Kohling R, Heinemann U, Theis M, Willecke K, Steinhauser C. The impact of astrocytic gap junctional coupling on potassium buffering in the hippocampus. J Neurosci. 2006; 26(20): 5438–5447. [PubMed: 16707796]

Wang W, Gao XF, Xiao L, Xiang ZH, He C. K(V)7/KCNQ channels are functionally expressed in oligodendrocyte progenitor cells. PLoS One. 2011; 6(7):e21792. [PubMed: 21750731]

Wang YH, Li YC, Huo SJ, Yin ZQ. Alpha-crystallin promotes rat olfactory ensheathing cells survival and proliferation through regulation of PI3K/Akt/mTOR signaling pathways. Neurosci Lett. 2012; 531(2):170–175. [PubMed: 23142719]

Watanabe K, Kondo K, Takeuchi N, Nibu K, Kaga K. Age-related changes in cell density and the proliferation rate of olfactory ensheathing cells in the lamina propria of postnatal mouse olfactory mucosa. Brain Res. 2006; 1116(1):82–92. [PubMed: 16952341]

Yan H, Bunge MB, Wood PM, Plant GW. Mitogenic response of adult rat olfactory ensheathing glia to four growth factors. Glia. 2001; 33(4):334–342. [PubMed: 11246232]

Main points

This is the first characterization of olfactory ensheathing glia potassium currents, showing variable expression of inward and delayed rectifier potassium channels, and gap junction channels. Diversity relates in part to location of cells in different layers of the olfactory bulb.

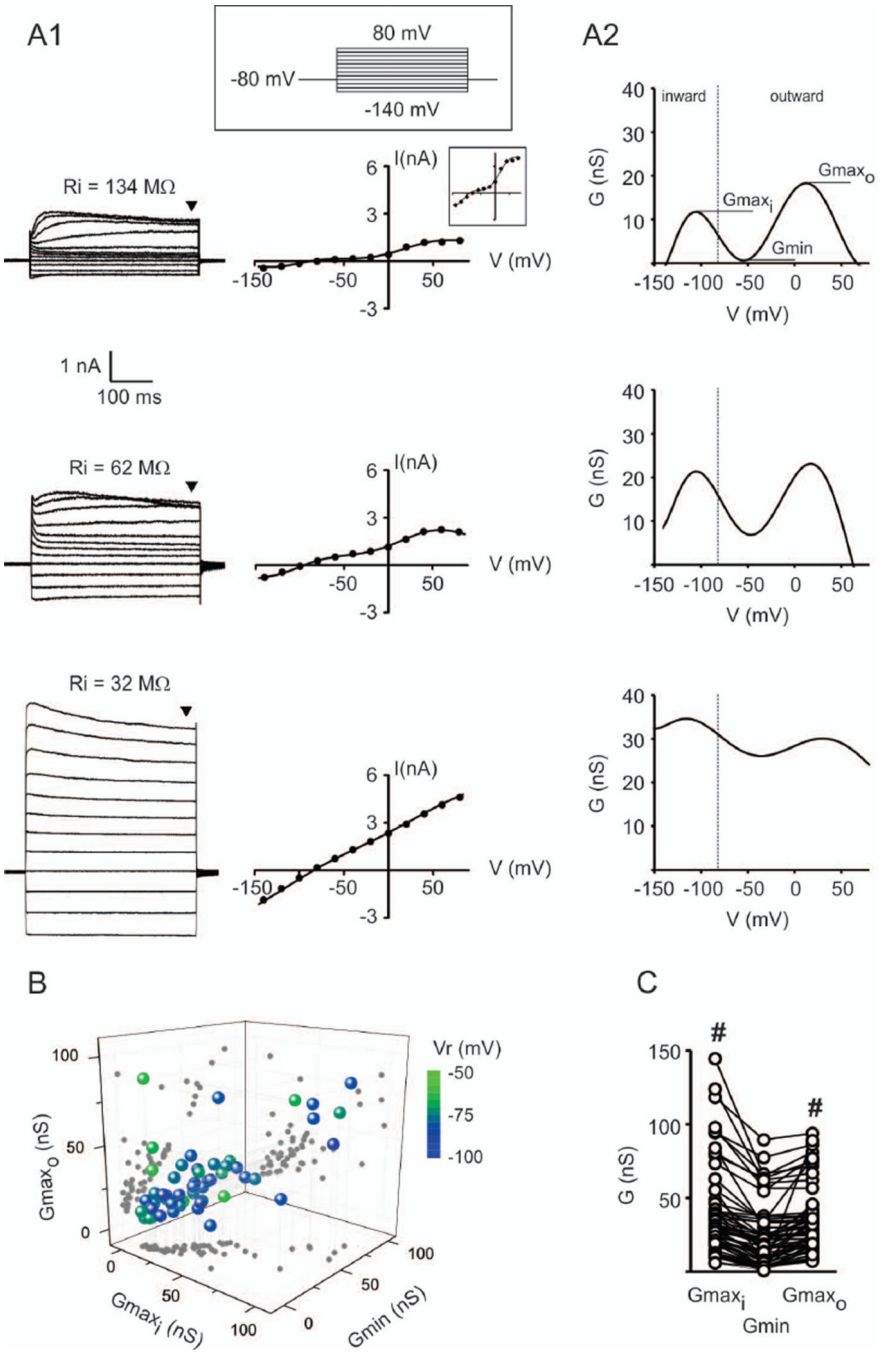

Fig. 1.

Diversity of OEC membrane current profiles. **A1:** Whole cell currents (left) of OECs subjected to a series of voltage steps (−140 to 80 mV, Δ20 mV). Examples of cells with high (*top*), intermediate (*middle*) and low (*bottom*) R_i values. I/V curves are shown at the right. Inset: expanded scale (tick marks: 1 nA, 50 mV). **A2:** Derivatives of the I/V curves (*dI/dVm*) shown in A1. The top graph indicates maxima ($Gmax_i$, $Gmax_o$) and minima (Gmin) of interest. The vertical line separates the range of voltages eliciting inward (left) or outward (right) currents. **B:** 3D representation of $Gmax_i$, Gmin and $Gmax_o$. Each symbol represents a

different OEC and 2D projections are in gray symbols. V_r is color coded (n=56). **C:** $Gmax_i$, Gmin and $Gmax_o$ for the same OEC sample shown in B. Values corresponding to the same OEC are connected with lines. # $p<0.05$, compared to Gmin (Friedman test, n=56 cells).

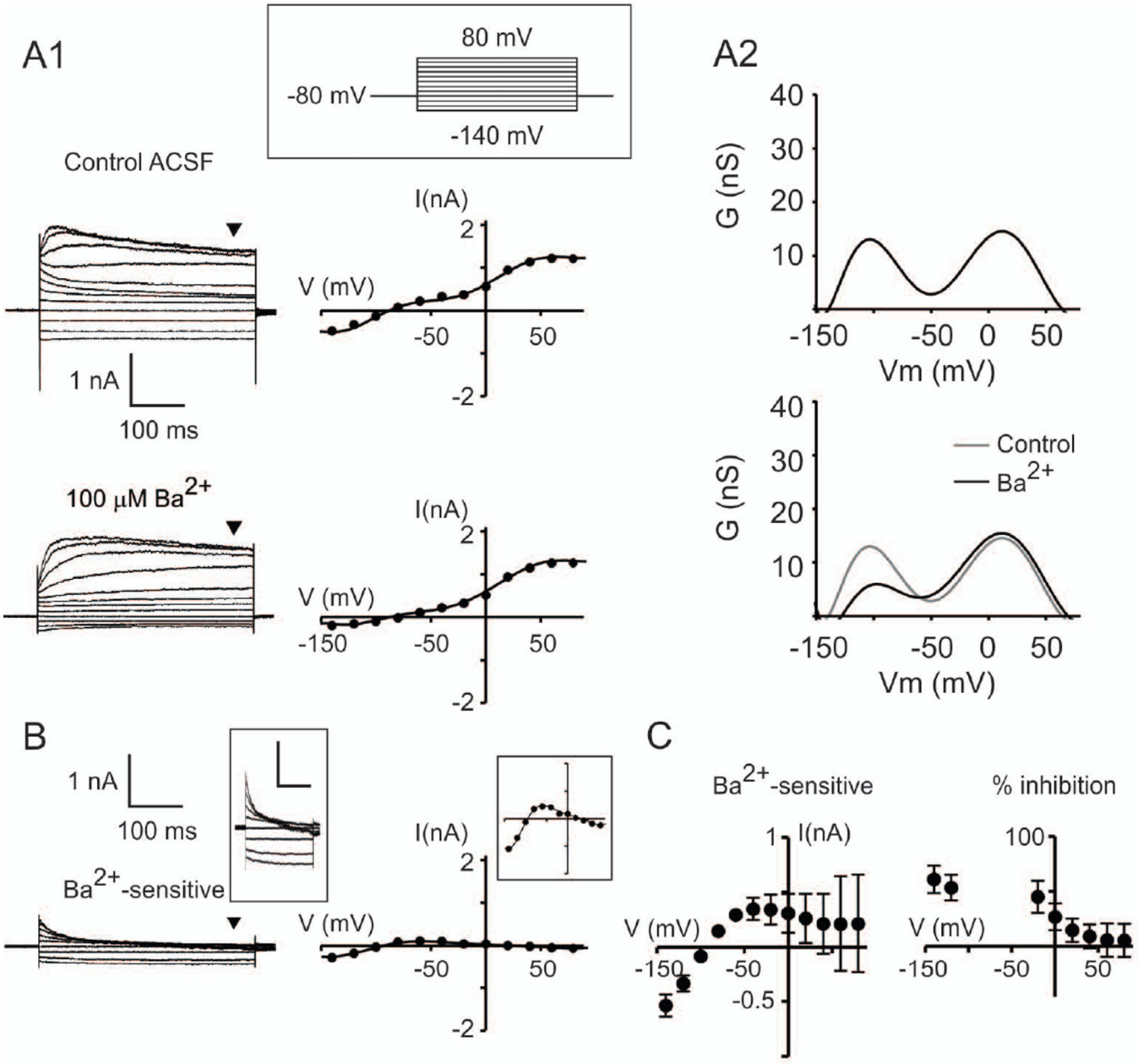

Fig. 2.

Ba^{2+} blocks a hyperpolarization-activated inward current of OECs. **A1:** Whole cell currents (left) of an OEC subjected to a series of voltage steps (−140 to 80 mV, Δ20 mV) in control (top) and with 100 μM Ba^{2+} (bottom). I/V curves are shown at the right. **A2:** Conductance as a function of Vm for the curves shown in A1. The bottom graph shows the control conductance (gray) overimposed to the conductance in the presence of Ba^{2+} (black). **B:** Ba^{2+}-sensitive component for the OEC shown in A1, with the I/V curve at the right. Insets: expanded scale (scale bars: 0.5 nA, 200 ms; tick marks: 0.25 nA, 50 mV). **C:** Average I/V curve of the Ba^{2+}-sensitive current, normalized to the maximum inward current in control

conditions (left, n=8) and average percent inhibition of the total current as a function of Vm (right, n=8).

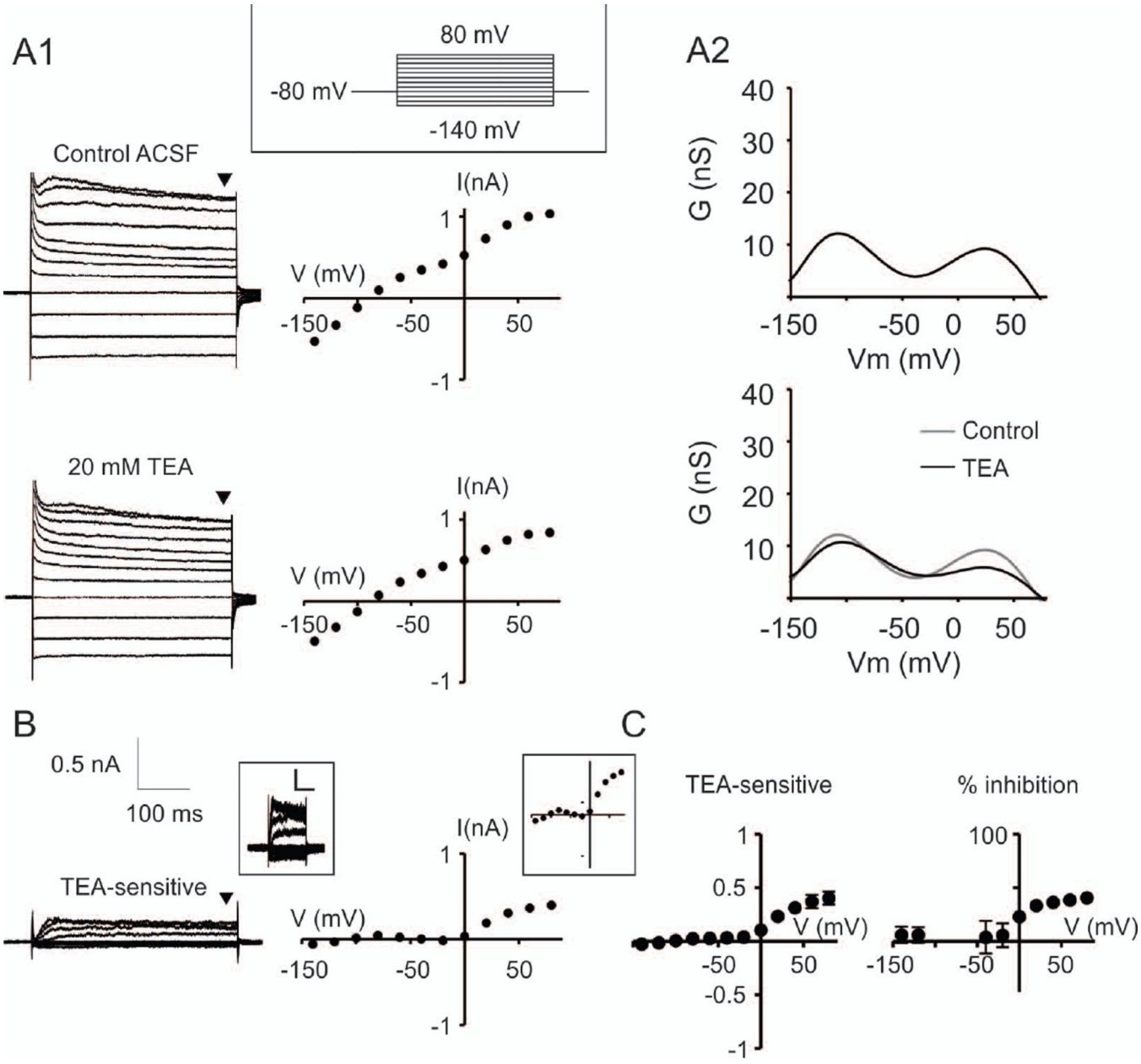

Fig. 3.

TEA blocks depolarization-activated outward currents of OECs. **A1:** Representative whole cell currents (left) of an OEC subjected to a series of voltage steps (−140 to 80 mV, Δ20 mV) in control (top) and with 20 mM TEA (bottom). I/V curves are shown at the right. **A2:** Derivatives of the I/V curves shown in A1. The bottom graph shows the control derivative (gray) overimposed to the derivative in the presence of TEA (black). **B:** TEA-sensitive component of the OEC shown in A1, with the I/V curve at the right. Inset: expanded scale for better appreciation of outward rectification (scale bars: 0.2 nA, 200 ms; tick marks: 0.25 nA, 50 mV). **C:** Average I/V curve of the TEA-sensitive current, normalized to the maximum outward current in control conditions (left, n=10) and average percent inhibition of the total current as a function of Vm (right, n=10).

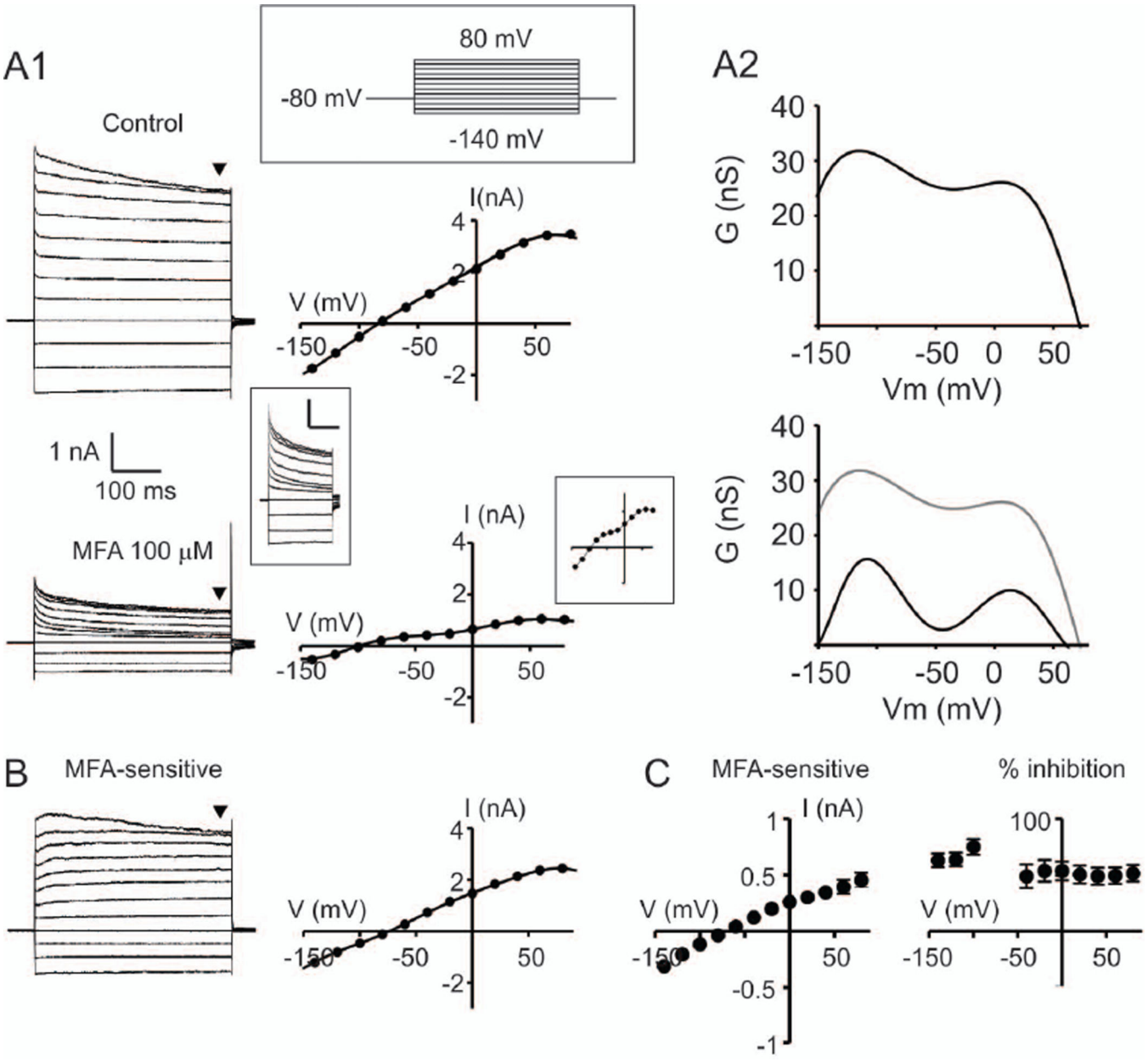

Fig. 4.

MFA blocks ohmic currents of OECs. **A1:** Representative whole cell currents (left) of an OEC subjected to a series of voltage steps (−140 to 80 mV, Δ20 mV) in control (top) and in the presence of 100 μM MFA (bottom). I/V curves are shown at the right. **A2:** Derivatives of the I/V curves shown in A1. The bottom graph shows the control derivative (gray) overimposed to the derivative in the presence of MFA (black). **B:** MFA-sensitive component of the OEC shown in A1, with the I/V curve at the right. **C:** Average I/V curve of the TEA-sensitive current, normalized to the maximum outward current in control conditions (left, n=12) and average percent inhibition of the total current as a function of Vm (right, n=12).

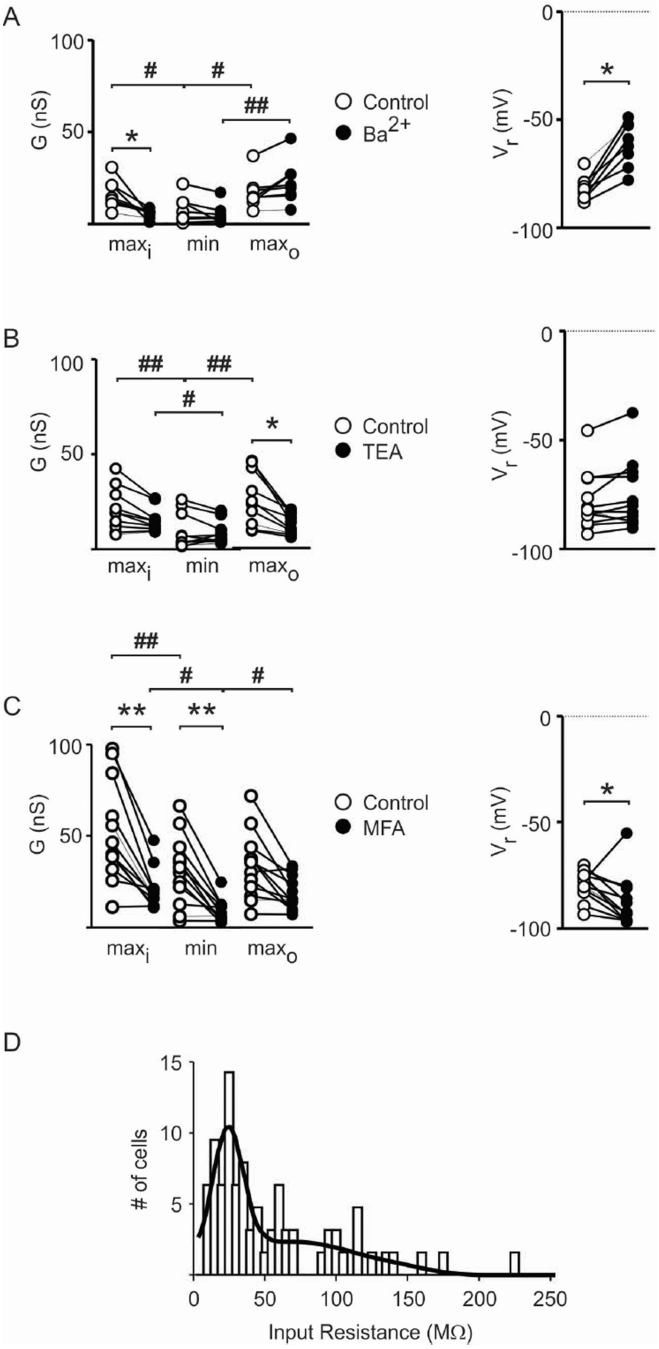

Fig. 5.

Effects of channel blockers on conductance and linearity of the I/V curve. The graphs show $Gmax_i$, Gmin and $Gmax_o$ (left) or V_r (right) before (white symbols) and after (black symbols) treatment with 100 μM Ba^{2+} (**A**), 20 mM TEA (**B**) or 100 μM MFA (**C**). Each symbol corresponds to a different OEC. Statistical comparisons: Bonferroni posttests in a 2-way repeated measures-ANOVA with Treatment and Conductance of interest (COI) as factors. **A:** * $p<0.05$, Ba^{2+} vs. control; # $p<0.05$, ## $p<0.001$, Gmax vs. Gmin; (effect of COI: $p<0.001$; interaction: $p<0.001$, n=8). **B:** * $p<0.01$, TEA vs. control; # $p<0.05$, ##

p<0.001, Gmax vs. Gmin; (effect of COI: p<0.001; interaction: p<0.01, n=10). **C:** * p<0.05, ** p<0.001, MFA vs. control; # p<0.05, ## p<0.001, Gmax vs. Gmin; (effect of Treatment: p<0.01; effect of COI: p<0.001; interaction: p<0.01 n=12). **D:** Histogram of OEC R_i values. Black line: preferred model of a comparison of non-linear regression models (Gaussian versus sum of two Gaussian functions, *p<0.001*, R^2=0.782, n=63)

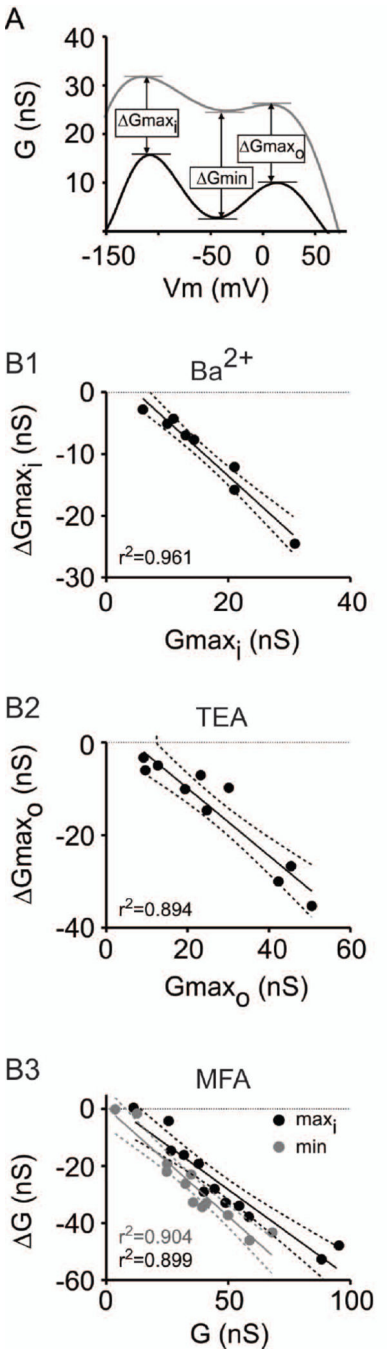

Fig. 6.

The degree of inhibition by channel blockers depended on the initial conductance of OECs. **A:** Same graph of G vs. Vm shown in Figure 1A2 indicating how changes in conductance were measured for each voltage range of interest. **B:** Change in conductance (ΔG) produced by each blocker vs. initial conductance (G) at the same voltage range for a subsample of OECs treated with 100 μM Ba^{2+} (**B1**), 20 mM TEA (**B2**) or 100 μM MFA (**B3**). Solid lines: linear regression analyses; broken lines: 95% confidence interval.

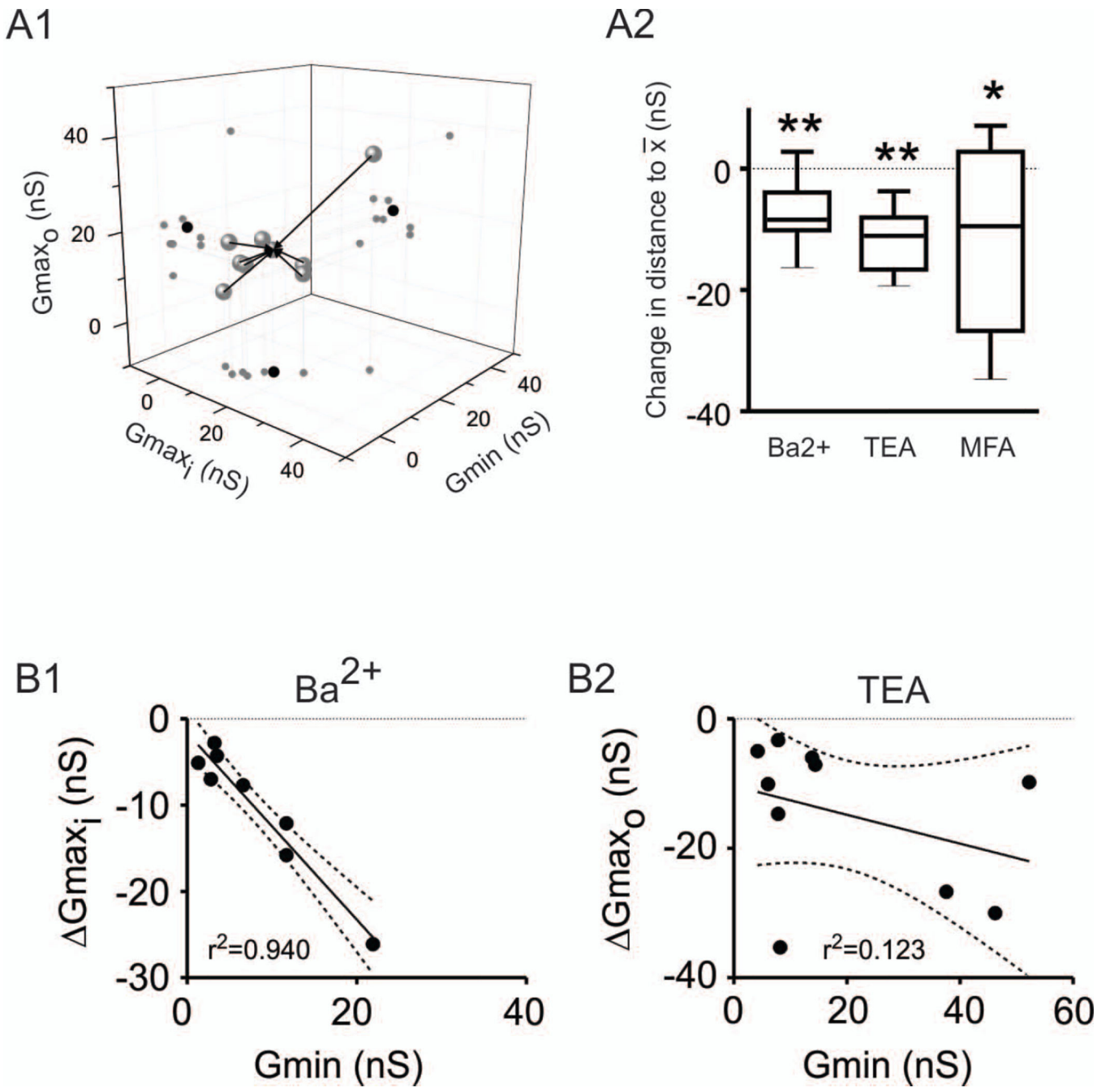

Fig. 7.

K_{ir}, K_{DR} and GJ channels contributed to variability of biophysical properties of OECs. **A1:** Same data as in Figure S5A (left) showing how distance to the mean was measured. **A2:** Change in distance to the 3D mean value produced by each channel blocker. * $p<0.05$, ** $p<0.01$, Wilcoxon test, comparing to a hypothetical value of zero. **B:** Change in conductance (ΔG) produced by each blocker vs. Gmin for a subsample of OECs treated with 100 μM Ba^{2+} (**B1**) or 20 mM TEA (**B2**). Solid lines: linear regression analyses; broken lines: 95% confidence interval.

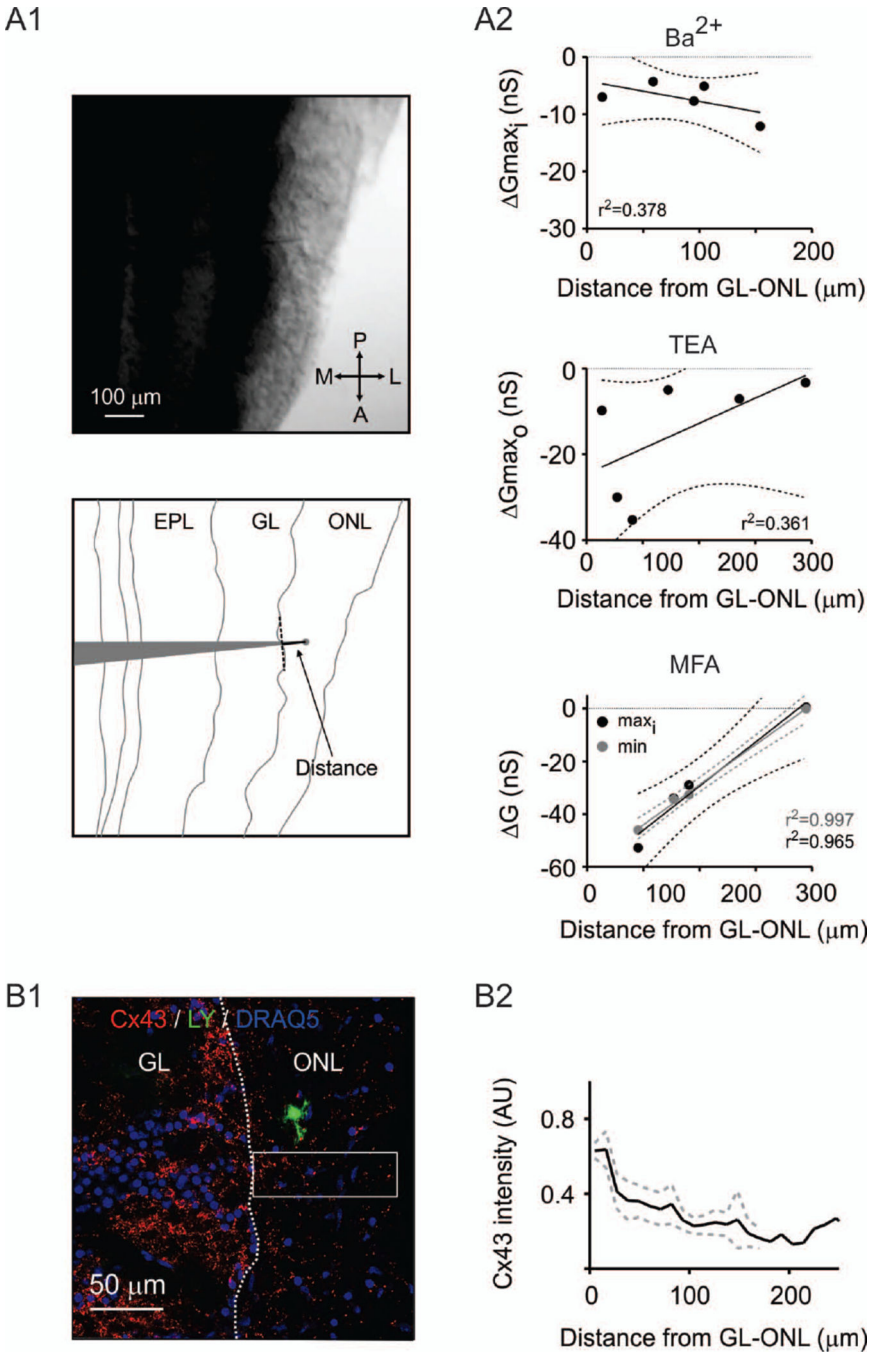

Fig. 8.

GJ channels are regionally expressed in the ONL. **A1:** Representative image under DIC illumination showing the layers of the OB and the location of the recording pipette (top). The bottom drawing illustrates the procedure to measure distance from the recorded OECs to the inner ONL border. **A2:** Sensitivity to each blocker versus location of OECs. Each symbol represents a cell; solid lines: linear regression analyses; dotted lines: 95% confidence interval. **B1:** representative OB slice showing a lucifer yellow-filled OEC (green), immunoreactivity for Cx43 (red) and nuclear stain (blue). Dotted line: inner ONL

border. Rectangular selection: representative region of interest (ROI) used for quantification. **B2:** Average plot profile representing the intensity of Cx43 immunoreactivity as a function of distance from the inner ONL border. Dotted lines: SEM (n=4).